AIP | Journal of Applied Physics

Effects of nonuniform exchange and magnetostatic interactions on the determination of intrinsic switching field distributions

Yang Liu, Ondrej Hovorka, Andreas Berger, and Karin A. Dahmen

Citation: J. Appl. Phys. **105**, 123905 (2009); doi: 10.1063/1.3149696
View online: http://dx.doi.org/10.1063/1.3149696
View Table of Contents: http://jap.aip.org/resource/1/JAPIAU/v105/i12
Published by the American Institute of Physics.

Effects of nonuniform exchange and magnetostatic interactions on the determination of intrinsic switching field distributions

Yang Liu,[1,a)] Ondrej Hovorka,[2] Andreas Berger,[2] and Karin A. Dahmen[1]
[1]*Department of Physics, University of Illinois at Urbana-Champaign, Urbana, Illinois 61801, USA*
[2]*CIC nanoGUNE Consolider, Donostia, San Sebastian 20009, Spain*

(Received 23 February 2009; accepted 10 May 2009; published online 17 June 2009)

A systematic numerical study is performed on the $\Delta H(M,\Delta M)$ method and its ability to determine the intrinsic switching field distributions of perpendicular recording media in the presence of locally varying intergranular exchange and magnetostatic interactions. It is found by means of evaluating various reliability measures that the overall robustness of the $\Delta H(M,\Delta M)$ method is only slightly reduced due to the presence of randomness in both the exchange and magnetostatic interactions, at least within the parameter range that is relevant for typical recording media.
 [DOI: 10.1063/1.3149696]

I. INTRODUCTION

For granular magnetic materials such as magnetic recording media, the determination of intrinsic properties from macroscopic measurements is complicated by the presence of intergranular exchange and magnetostatic interactions.[1] This issue is particularly relevant for perpendicular recording media (PRM), due to the fact that the strength of the interactions is much larger than in the previously used longitudinal recording media.[2] Recently, it has been shown that the microstructural disorder and the resulting randomness in exchange and magnetostatic intergranular interactions have a detrimental effect on the performance of PRM.[1,3,4]

In real granular materials, the randomness in the exchange couplings arises from irregularities at the grain boundaries, while the randomness in the magnetostatic couplings results from the distribution of locations and volumes of the grains. Therefore, it is important to find a self-consistent approach to generating a realistic distribution of grains and the corresponding intergranular interactions. The purpose of the present paper is twofold. First, the aim is to develop a realistic model of PRM that self-consistently accounts for locally varying random interactions, while still allowing for the macroscopic hysteresis loop description of PRM. Second, the so developed model is subsequently used to address the question: to what extent can the presence of random interactions influence the proper determination of microscopic materials information, such as the intrinsic switching field distribution (SFD) $D(H_S)$?

While many hysteresis-loop-measurement based techniques have been developed for extracting the $D(H_S)$ in PRM, the recently devised $\Delta H(M,\Delta M)$ method has been found to be most accurate and reliable, as well as easy to implement.[2,5–9] This method measures the field difference ΔH at constant magnetization M between the major hysteresis loop and a number of recoil curves, which each start at a certain distance ΔM away from the saturation M_S. Within the mean-field approximation, the functional dependency of ΔH can be written as

$$\Delta H(M,\Delta M) = I^{-1}\left(\frac{1-M}{2}\right) - I^{-1}\left(\frac{1-M-\Delta M}{2}\right), \qquad (1)$$

where I^{-1} is the inverse of the field integral $I(x) = \int_{-\infty}^{x} D(H_S)dH_S$ of the intrinsic SFD. Within the mean-field approximation, the field difference ΔH is independent from the grain interactions, which allows for a direct experimental access to determining $D(H_S)$. For certain parameterized distribution functions, one can derive analytic expressions for $D(H_S)$. For example, for a Gaussian distribution of width σ, one finds

$$\Delta H_G(M,\Delta M) = \sqrt{2}\sigma[\mathrm{erf}^{-1}(M+\Delta M) - \mathrm{erf}^{-1}(M)]. \qquad (2)$$

Details of this method and the analysis formalism have been described previously.[2,5,7] This method has two main advantages over comparable methods: (1) it allows for the determination of the entire $D(H_S)$ distribution and its functional form and not just a single characteristic parameter.[2,5] (2) Its reliability can be verified by a straightforward redundancy test of the experimental data.[7,9]

In the present work, we numerically test the ability of the $\Delta H(M,\Delta M)$ method with an improved interacting random hysteron model of PRM, which self-consistently accounts for the randomness in the intergranular exchange and magnetostatic interactions and the volume distributions of grains. It is found that increasing the randomness of the exchange or magnetostatic interactions within the range of a typical recording media reduces the reliability of the method only slightly and in a well controlled fashion. In all cases, strong correlations are observed between the reliability measures of this method and a self-consistency-check of the data sets, which is based upon the straightforward redundancy measure. This suggests that the latter can be utilized as an efficient criterion to decide if a complete data analysis is warranted or not, corroborating our earlier result.[9]

II. MODEL

To model PRM and study the reliability of the $\Delta H(M,\Delta M)$ method, a two-dimensional (2D) interacting *random* hysteron model has been used in previous studies.[7,9]

[a)]Electronic mail: yangliu@illinois.edu.

In this model, each media grain is considered as a symmetric hysteron, which generates a rectangular hysteresis loop in an applied field H. The half width of the hysteresis loop is just the intrinsic switching field H_S of this hysteron. It is further assumed that the magnetization of each hysteron exhibits values of ± 1 only and orients exactly along the applied field H and perpendicular to the recording layer (representing high-anisotropy materials). In the planar geometry of thin films with perfectly aligned perpendicular magnetization, dipolar effects cause an effective interaction that is antiferromagnetic (AFM) in its nature. The PRM is then represented by a square or triangular lattice of hysterons with periodic boundary conditions, described by Hamiltonian

$$\mathcal{H} = -J_{\mathrm{ex}} \sum_{\langle i,j \rangle} S_i S_j + J_{\mathrm{dp}} \sum_{i \neq j} \frac{S_i S_j}{\tilde{r}_{ij}^3} - \sum_i [H + \mathrm{sgn}(S_i) H_{S_i}] S_i, \tag{3}$$

with $\tilde{r}_{ij} = r_{ij}/a$ the reduced distance between hysteron i and j measured in units of lattice spacing a and $\mathrm{sgn}(x)$ the signum function. Here, the first term represents the ferromagnetic (FM) nearest neighbors interaction term quantified by means of the exchange coupling constant J_{ex}. The second term describes the dipolar interactions of strength J_{dp} among all hysteron pairs. The third term accounts for the effect of the external field and the intrinsic switching field of hysterons.

This model has been demonstrated to be very useful for understanding the applicability of the $\Delta H(M, \Delta M)$ method to PRM.[9] However, it has substantial deficiencies. First, mapping grains to structuralist hysterons is of course the simplest mathematical construction, in which any effects due to the grain volume distributions are completely ignored. Second, the assumption of uniform exchange and dipolar couplings (J_{ex} and J_{dp}) is a substantial simplification of the real material structures. Due to microstructural disorder, such as irregularities at the grain boundaries, (or random locations and volumes of grains), there is a distribution of exchange (or magnetostatic) couplings between grains. Third, the dipole approximation is satisfactory for grains which are far away from each other. For grains which are close to each other, the dipole approximation will significantly overestimate the magnetostatic interactions, as reported in the literature.[10,11] Considering all these deficiencies and to systematically study the effect of nonuniform exchange and magnetostatic interactions on the reliability of the $\Delta H(M, \Delta M)$ method, we have generalized the above simple model [Eq. (3)] in the following three aspects.

A. Nonuniform exchange interactions

For realistic PRM materials, the randomness in the intergranular exchange couplings is determined mostly by the quality of the grain boundaries (or by an additional layer introducing a well-defined amount of intergranular interactions), while the randomness in the magnetostatic interactions is determined by the grain volume distribution. Thus for all practical purposes, it is reasonable to view the probability distributions of the intergranular exchange and magnetostatic couplings as mutually uncorrelated. Therefore, for the modeling purposes, the two distributions can be generated using independent processes.

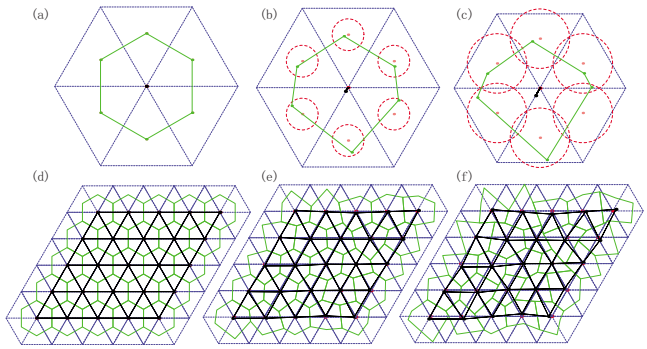

FIG. 1. (Color online) RHT: tuning the parameter P varies the shape of a single grain and causes a nonuniform grain volume distribution for the grain assembly. [(a) and (d)] $P=0$; [(b) and (e)] $P=0.6$; and [(c) and (f)] $P=1.2$. The grains are shown in green hexagons. The embedded triangular lattice of grains with periodic boundary conditions is shown in blue dashed lines. The bonds between lattice sites (or grain centroids) and their nearest neighbors are shown in blue (or black) solid lines. In [(b) and (c)], the red dashed circle shows the permitted region of the grain vertices with radius $r = Pa/(2\sqrt{3})$. Here $a=1$ is the lattice spacing. For $P>0$, the grain centroids (black dots) become deviating from the lattice sites (red dots). Only in the regular hexagonal tiling case ($P=0$), as shown in [(a) and (d)], the grain centroids match the lattice sites.

Correspondingly, we introduce randomness in the exchange couplings by simply choosing random bonds J_{ex}^{ij} from a Gaussian distribution with mean $\langle J_{\mathrm{ex}}^{ij} \rangle \equiv J_{\mathrm{ex}}$ and standard deviation $\sigma(J_{\mathrm{ex}}^{ij}) \equiv R_{\mathrm{ex}} J_{\mathrm{ex}}$. The relative width of the random bond distribution R_{ex} will be called the randomness in the exchange couplings. The bond index $b=(ij)$ runs from 1 to $NZ/2$ with Z the coordination number of the embedded lattice. To make a good approximation of actual media structures in which grains typically have coordination numbers of 5 and 6, we choose a triangular lattice of grains with constant coordination number $Z=6$.

B. Nonuniform magnetostatic interactions

Due to the nonlocal nature of magnetostatic interactions, a self-consistent generation of random coupling constants J_{ms}^{ij} is a nontrivial task. In a first step, we represent the volume of a grain by a hexagonal prism with a side length $a/\sqrt{3}$ and height d [Figs. 1(a) and 4(b)]. Thus the grains form a 2D assembly of thickness d with grains arranged on a triangular lattice of spacing a [Figs. 1(d) and 4(a)]. Then we randomize volumes of grains by a random hexagonal tiling (RHT) process (see below), in which the plane of the triangular lattice is tiled with randomly irregular hexagons on each lattice site [Fig. 1(e)]. The height d remains the same for all grains. Note that this process guarantees that every grain has exactly six neighbors, which complies with the definition of nonuniform exchange interactions above.

The RHT process is illustrated in Figs. 1(a)–1(c). First we assume a regular tiling case and draw a circle of radius $r = Pa/(2\sqrt{3})$ around every vertex of all the regular hexagons. Then we randomly generate a point inside every such circle. These points define the locations of the vertices of the randomized hexagons. The randomized volume v_i of grain i is

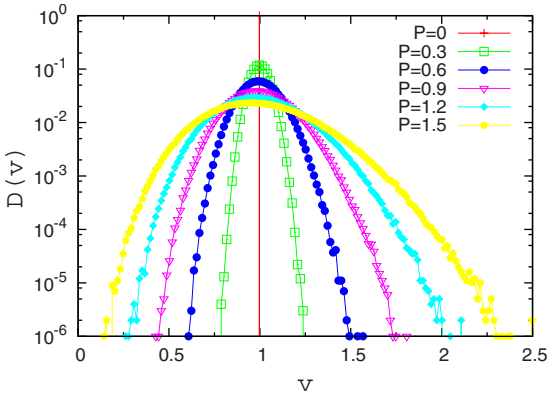

FIG. 2. (Color online) The normalized grain volume distribution $D(v)$ for different RHT parameter values for a triangular lattice with $L=1000$ and $N=10^6$ grains. Here v is in units of the mean grain volume v_0.

calculated by multiplying the area of the hexagon A_i by the height d. The extent of randomness can be controlled by the tuning parameter P, where $P=0$ corresponds to the regular hexagonal tiling case. As shown in Figs. 1(a)–1(c), with increasing P, the grain becomes more and more irregular. Figures 1(d)–1(f) illustrate the corresponding deformation of the entire lattice.

It is interesting to study the correlation between the tuning parameter P and the grain volume distribution $D(v_i)$ generated by the described RHT. First of all, we plot the $D(v_i)$ obtained from RHT at different P values (see Fig. 2). Note that here we have normalized the grain volume v_i to the value of the regular tiling case which is just $v_0=\sqrt{3}a^2d/2$. For $P=0$, $D(v_i)$ corresponds to a δ-function. As P increases, we see that $D(v_i)$ becomes broader and more asymmetrical. Second, the tuning parameter P is correlated with the characteristics (moments) of the grain volume distribution $D(v_i)$, e.g., the mean, variance, and skewness. To see this, we plot the moments of $D(v_i)$ as functions of P in Fig. 3. The first moment, i.e., the mean value $\langle v\rangle$, is always equal to unity (in units of v_0) no matter how randomly the hexagons are drawn, see Fig. 3(a). This is done by keeping the number of grains

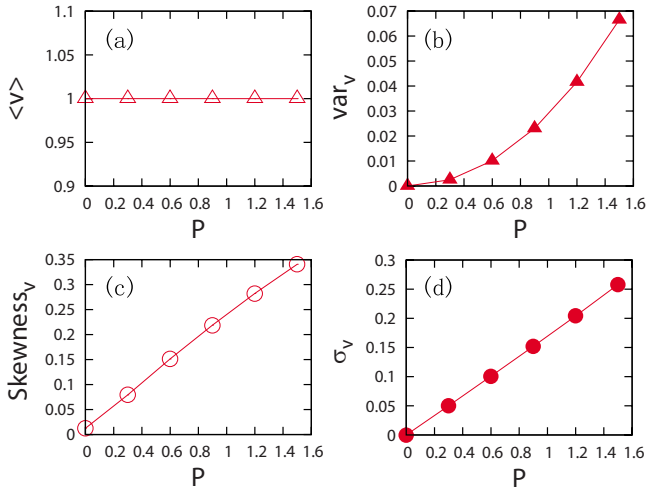

FIG. 3. (Color online) The mean, variance, skewness, and standard deviation of the grain volume distribution $D(v)$ as functions of the RHT parameter P on a triangular lattice with $L=1000$ and P grains. Here v is in units of the mean grain volume v_0.

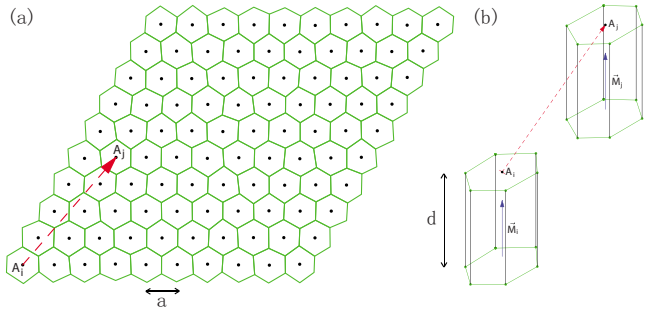

FIG. 4. (Color online) (a) A 2D grain assembly (with $L=10$ and $N=100$) obtained by RHT with the tuning parameter $P=0.2$, which results in a grain volume distribution $D(v)$ with $\sigma(v)\approx 0.035v_0$. A_i and A_j denote surface areas of grain i and j. (b) Schematic 3D view of the chosen grain pair.

and the total area of the grain assembly constant in the RHT process. (Note that in our calculations, we use periodic boundary conditions, so that the total area is actually an infinite sheet. For the central simulation cell, the number of grains and the total area of the grain assembly are kept constant so that the average grain volume is the same as we tune P in the RHT process.) We want to keep $\langle v\rangle$ the same as we systematically tune P because otherwise the total magnetostatic energy varies, which is an effect we want to isolate and only tune by means of the corresponding coupling constant. The second moment (variance) of the distribution follows parabolic behavior [Fig. 3(b)]. To confirm this, we also plot the standard deviation $\sigma(v_i)$ as a function of P. A straight line $\sigma(v_i)=0.17P$ (in units of v_0) can fit the data very well [see Fig. 3(d)]. For the third moment, i.e., the skewness, a positive value increases roughly linearly with P, which indicates that the $D(v_i)$ becomes more asymmetric with increasing P as seen in Fig. 3(c).

A self-consistent distribution of the magnetostatic couplings $D(J_{\rm ms}^{ij})$ is then naturally obtained by setting $J_{\rm ms}^{ij}=J_{\rm ms}v_iv_j/v_0^2$ with $J_{\rm ms}$ the magnetostatic coupling strength in the $P=0$ limit, i.e., no randomness in the grain volume distribution: $v_i=v_j=v_0$. Due to the long-range feature of the magnetostatic interaction, the index (ij) (with $i\neq j$) denotes here all the grain pairs in the system.

C. Magnetostatic versus dipolar picture

To calculate the intergranular magnetostatic interactions, we conduct the following procedures. Suppose we have a grain assembly with a volume distribution $D(v_i)$ obtained by RHT, as shown in Fig. 4(a).

Generally, the magnetic scalar potential Φ_M of a given body, e.g., a media grain, with known magnetization $\boldsymbol{M}$ is given by

$$\Phi_M(\boldsymbol{r})=-\int_V \frac{\nabla\cdot\boldsymbol{M}(\boldsymbol{r}')}{|\boldsymbol{r}-\boldsymbol{r}'|}dV'+\oint_A \frac{\hat{\boldsymbol{n}}\cdot\boldsymbol{M}(\boldsymbol{r}')}{|\boldsymbol{r}-\boldsymbol{r}'|}dA', \tag{4}$$

in the Gaussian cgs system of units. Since in our model, we assume uniform magnetization inside each grain, the volume integral of the first term vanishes. Furthermore, since we consider the high anisotropy limit where magnetization of each grain can be aligned only along the z-axis, only the top and bottom surfaces will contribute to the surface integral of

the second term. We define the magnetostatic field produced by grain j as $\boldsymbol{H}_{M_j}(\boldsymbol{r})=-\nabla\Phi_{M_j}(\boldsymbol{r})$. The magnetostatic energy between grain i and grain j can then be written as

$$U_{\rm ms}^{ij}=-\frac{1}{2}\int_{V_i}\boldsymbol{M}_i\cdot\boldsymbol{H}_{M_j}dV=\frac{1}{2}\boldsymbol{M}_i\cdot\int_{V_i}\nabla\Phi_{M_j}dV$$
$$=\frac{1}{2}\boldsymbol{M}_i\cdot\oint_{A_i}\Phi_{M_j}\hat{\boldsymbol{n}}_i dA$$
$$=\frac{1}{2}\oint_{A_i}\oint_{A_j}\frac{(\hat{\boldsymbol{n}}_i\cdot\boldsymbol{M}_i)(\hat{\boldsymbol{n}}_j\cdot\boldsymbol{M}_j)}{|\boldsymbol{r}-\boldsymbol{r}'|}dA'dA. \quad (5)$$

The coordinates of points in the top/bottom surface of grain i and grain j are $(x,y,\pm d/2)$ and $(x',y',\pm d/2)$, respectively. Then it is easy to check that

$$U_{\rm ms}^{ij}=\frac{1}{2}S_iS_jM_0^2\mathcal{I}(\boldsymbol{r}_i,\boldsymbol{r}_j;d). \quad (6)$$

Here, $\boldsymbol{M}_i=S_iM_0\hat{\boldsymbol{z}}$, $\boldsymbol{M}_j=S_jM_0\hat{\boldsymbol{z}}$ with $S_i,S_j=\pm1$ and M_0 is a material parameter. The integral

$$\mathcal{I}(\boldsymbol{r}_i,\boldsymbol{r}_j;d)=\int\int_{A_i}dxdy\int\int_{A_j}dx'dy'2\cdot\left[\frac{1}{\sqrt{(x-x')^2+(y-y')^2}}-\frac{1}{\sqrt{(x-x')^2+(y-y')^2+d^2}}\right] \quad (7)$$

is evaluated along the top surfaces (A_i and A_j) of the two grains with centroid coordinates $\boldsymbol{r}_i=(x_i,y_i,d/2)$ and $\boldsymbol{r}_j=(x_j,y_j,d/2)$, respectively.

In the limit that the two grains are far away from each other $\sqrt{(x_i-x_j)^2+(y_i-y_j)^2}\equiv r_{ij}\gg d$, the above integral can be calculated as

$$\mathcal{I}(\boldsymbol{r}_i,\boldsymbol{r}_j;d)\approx A_iA_j2\left(\frac{1}{r_{ij}}-\frac{1}{\sqrt{r_{ij}^2+d^2}}\right)\approx\frac{A_iA_jd^2}{r_{ij}^3},$$

so that

$$U_{\rm ms}^{ij}\approx\frac{M_0^2d^2A_iA_j}{2a^3}\frac{S_iS_j}{\tilde{r}_{ij}^3}\equiv J_{\rm ms}^{ij}\frac{S_iS_j}{\tilde{r}_{ij}^3}, \quad (8)$$

which is the dipole approximation. Here, $\tilde{r}_{ij}=r_{ij}/a$ is the reduced distance and $J_{\rm ms}^{ij}$ is naturally defined to be the magnetostatic coupling strength between grain i and j in the long distance limit

$$J_{\rm ms}^{ij}=\frac{M_0^2d^2A_iA_j}{2a^3}=J_{\rm ms}\frac{A_iA_j}{A_0^2}=J_{\rm ms}\frac{v_iv_j}{v_0^2}, \quad (9)$$

with $J_{\rm ms}=3M_0^2d^2a/8$ being the magnetostatic coupling strength in the regular hexagonal tiling case ($A_i=A_j=A_0=\sqrt{3a^2/2}$). It is easy to recognize that $J_{\rm ms}$ is just the dipolar coupling constant $J_{\rm dp}$ used in our previous study.[9]

Having the complete magnetostatic solution, it is now possible to calculate how good the dipole approximation is. In Fig. 5, we show the ratio between the integration result calculated from Eq. (6) and the dipole-approximation result calculated from Eq. (8) as a function of r_{ij} (the distance between the two grains' centroids), for various d and P.

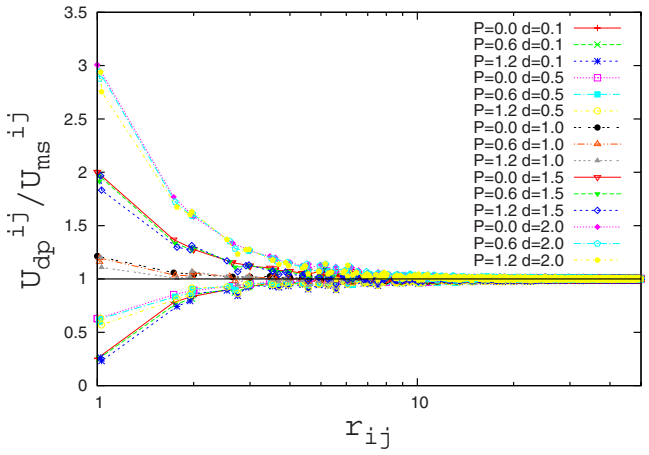

FIG. 5. (Color online) The ratio of the magnetostatic interactions between two grains calculated from Eqs. (8) and (6), respectively, as a function of the grain centroid distance r, at various d and P. $L=100$. Both r and d are in units of a.

One sees that for $d=2$, at $r=1$, the dipole approximation overestimates the magnetostatic interaction by almost 200%. While for $d=1$, at $r=1$, the dipole approximation overestimates the magnetostatic interaction by only 20%. Note that in a previous work,[11] the magnetostatic interaction energy of a three-dimensional (3D) array of FM cubes was calculated and the authors showed that the dipole approximation for nearest neighboring cubes overestimates the magnetostatic energy by more than 17%, which is comparable to our result given the fact that we are using different grain shapes.

We define r_c to be the cutoff distance beyond which the magnetostatic interaction can be calculated with the dipole approximation, i.e $U_{\rm dp}/U_{\rm ms}\approx1$ with less than 1% error. It is seen that r_c depends on d crucially. For example, for $d=1$, $r_c\approx4$; for $d=2$, $r_c\approx15$. (In our calculations, we set $d=2$ and $r_c=20$.) We also find that varying the RHT parameter P will not change r_c too much. This is demonstrated by the collapse of the curves with same d but different P values. To save computing time, we explicitly calculate the exact magnetostatic interactions only for grains with distance $r<r_c$, while for $r>r_c$ grains are still treated as in the dipole approximations.

Considering all the above changes, the model Hamiltonian of the interacting random hysteron model can now be written as

$$\mathcal{H}=-\sum_{\langle i,j\rangle}J_{\rm ex}^{ij}S_iS_j+\sum_{i\neq j}\frac{1}{2}M_0^2\mathcal{I}(\boldsymbol{r}_i,\boldsymbol{r}_j;d)S_iS_j-\sum_i[H+{\rm sgn}(S_i)H_{S_i}]\tilde{v}_iS_i, \quad (10)$$

with $\tilde{v}_i=v_i/\langle v\rangle$ being the scaled grain volume. Note that in the absence of randomness in the exchange and magnetostatic couplings and within the dipole approximation, the original Hamiltonian Eq. (3) is easily recovered from Eq. (10). The algorithm for the simulation of the major hysteresis loops and the corresponding recoil curves of this model is described in Ref. 7. For the numerical calculations of long-

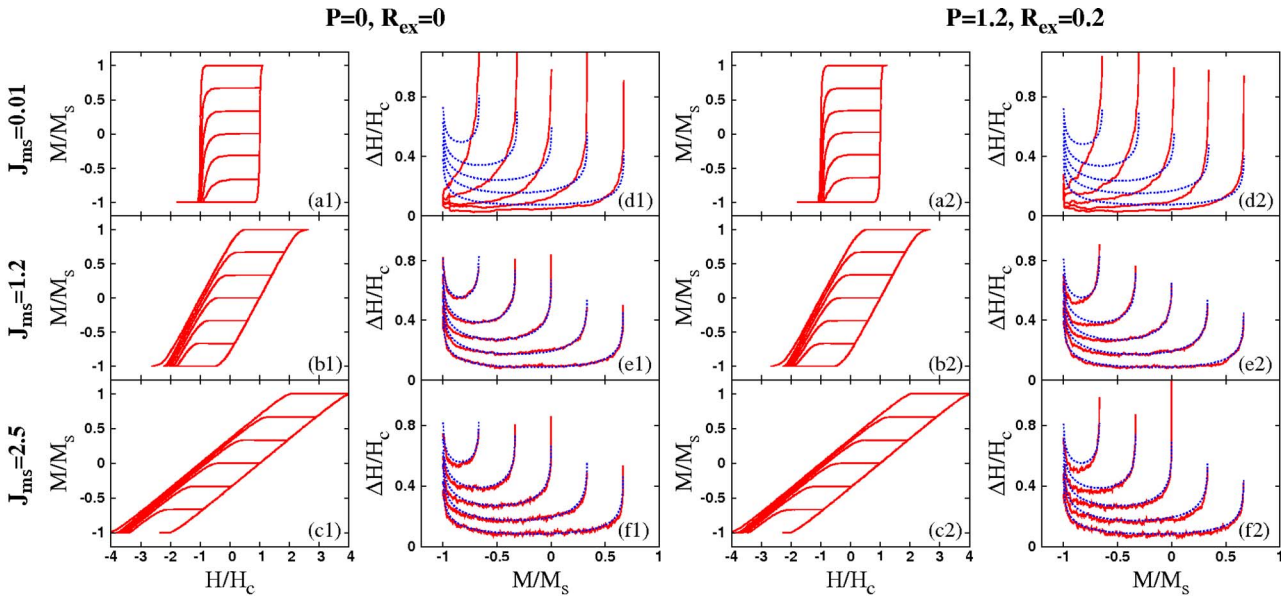

FIG. 6. (Color online) Using Gaussian $D(H_S)$ with width $\sigma=1.0$ to calculate the $M(H)$ and $\Delta H(M,\Delta M)$ curves on a 2D triangular lattice with $N=50^2$ grains and $J_{ex}=0.4$. (Columns 1 and 2) $P=0$, $R_{ex}=0$. (Columns 3 and 4) $P=1.2$, $R_{ex}=0.2$. Rows: $J_{ms}=0.01$, 1.2 and 2.5 from top to bottom. (Columns 1 and 3) $M(H)$ curves: main loop and five recoil curves. (Columns 2 and 4) $\Delta H(M,\Delta M)$ curves for the five recoil curves: (solid lines) numerical result; (dotted lines) mean-field approximation. Here M (or ΔM) is normalized to the saturation value $M_S=N$ and H (or ΔH) is normalized to the coercive field H_C.

range magnetostatic interactions in a system with periodic boundary conditions, we utilized the efficient Lekner formalism[12] as described in the Appendix.

III. RESULTS

For our numerical study of the $\Delta H(M,\Delta M)$ method's reliability, we assume a Gaussian distribution $D(H_S)$ of width σ for a 2D triangular lattice comprising of total N grains. Different systems sizes ranging from $N=50^2$ to 100^2 have been studied to estimate finite-size inaccuracies. In our model Hamiltonian, J_{ex}^{ij}, J_{ms}^{ij}, H, H_S, and σ all have dimensions of energy. Moreover, we set $\sigma=1$ to be the unit of energy.

The randomness in J_{ex}^{ij} is explicitly varied by tuning R_{ex}, the relative width of $D(J_{ex}^{ij})$. In our simulation, we tune R_{ex} from 0 up to 0.2. Note that for a Gaussian $D(J_{ex}^{ij})$ with positive mean, the ratio $R_{ex}=\sigma(J_{ex}^{ij})/\langle J_{ex}^{ij}\rangle \leq 0.2$ is generally small enough for probability of finding negative J_{ex}^{ij} to be negligible and, therefore, the exchange coupling is always FM in our simulations. The randomness in J_{ms}^{ij} is implicitly varied by tuning the RHT parameter P from 0 up to 1.2. Correspondingly, the relative width of the grain volume distribution $D(v)$, i.e., $R_v \equiv \sigma(v_i)/\langle v_i\rangle \sim 0.17P$, is tuned from 0 to 0.2. Note that $0 \leq R_{ex} \leq 0.2$ and $0 \leq R_v \leq 0.2$ are the parameter ranges that are relevant for typical recording media. We set the grain height $d=2a$. In calculating magnetostatic interactions, Eq. (6) is used for grains with distance $r<r_c=20a$ and Eq. (8) is used otherwise. We set the lattice spacing $a=1$ to be the unit of length.

For every pre-defined randomness parameter set (P,R_{ex}), we tune both J_{ms} and J_{ex}. Note that J_{ms} denotes the magnetostatic coupling strength between two grains in the long distance and $P=0$ limit. J_{ex} is the mean value of the introduced $D(J_{ex}^{ij})$. We calculate the complete set of $M(H)$-curves (both the saturation hysteresis loop and the recoil curves), from which the $\Delta H(M,\Delta M)$ data sets are then extracted.

A. *M*(*H*)

The results displayed in Fig. 6 show several specific examples. The simulated $M(H)$ curves are shown in the first and third column. It is clearly seen that increasing the strength of magnetostatic interaction J_{ms} shears the hysteresis loops substantially as expected. The second and forth column display the corresponding $\Delta H(M,\Delta M)$ curves. The solid lines are the numerically extracted results from the simulated $M(H)$ curves while the dotted lines denote the mean-field behavior according to the expression of $\Delta H_G(M,\Delta M)$. Comparing Fig. 6(d1), (e1), and (f1), we find that the magnetostatic interactions of intermediate strength make the system most mean-fieldlike and consequently the $\Delta H(M,\Delta M)$ method is most reliable there, corroborating our earlier result.[9] On the other hand, comparing Fig. 6(e1) with Fig. 6(e2), we find that the presence of randomness in J_{ms} and J_{ex} slightly change the system behavior from mean-fieldlike and consequently decreases the reliability of the $\Delta H(M,\Delta M)$ method somewhat.

B. Reliability measures

In our previous studies, we have introduced quantitative reliability measures to test the $\Delta H(M,\Delta M)$ method in a systematic way.[7,9] The reliability range of the mean-field approximation, upon which the $\Delta H(M,\Delta M)$ method is based, can be checked by means of a least-squares fit of $\Delta H_G(M,\Delta M)$ to the numerical data and a subsequent analysis of the conventional fit-quality measures, such as: (1) the square of the multiple correlation coefficient R^2 and (2) the percentage difference P_d between the fitting result and the input parameter σ. By definition, $R^2=1$ and $P_d=0$ would

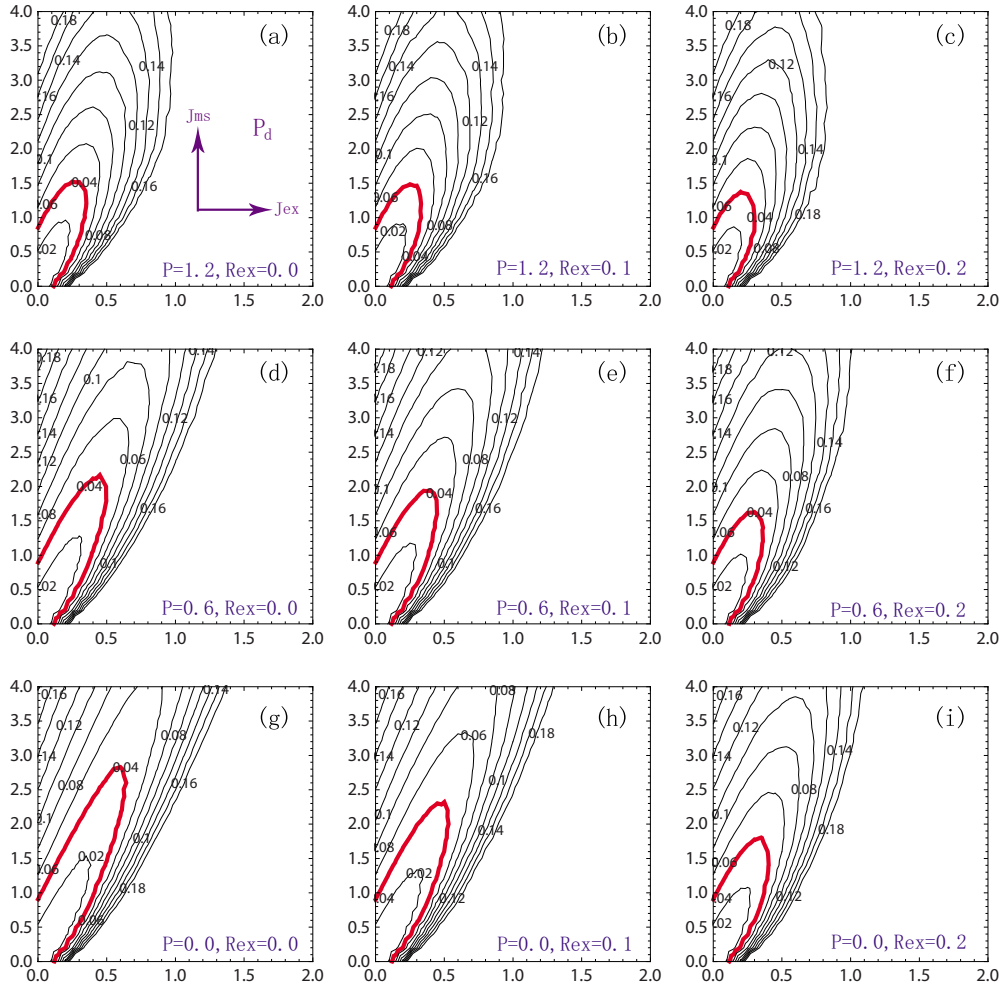

FIG. 7. (Color online) P and R_{ex} dependent contour plots of the reliability measure P_d. The critical contour with $P_d^c=-0.04$ is marked with thick solid lines.

correspond to perfect data fitting, i.e., the exactness of the mean-field limit. We calculated a least-squares fit to $\Delta H_G(M,\Delta M)$ for the numerically extracted $\Delta H(M,\Delta M)$ data for each parameter set of $(P,R_{\mathrm{ex}};J_{\mathrm{ms}},J_{\mathrm{ex}})$. From these fits, we then computed both P_d and R^2. The results are shown in contour plots (Figs. 7 and 8).

Besides the fit-quality measures R^2 and P_d, there is a self-consistency-check measure, which is based upon data redundancy in between multiple recoil curves.[7] One can test data for deviations from this redundancy by means of a quantity $r=\frac{1}{n}\Sigma_{i,j}\langle r_{ij}^2(M)\rangle^{1/2}$ with $r_{ij}(M)\equiv[\Delta H_i(M)+\Delta H_j(M-\Delta M_j)-\Delta H_i(M-\Delta M_j)-\Delta H_j(M-\Delta M_j+\Delta M_i)]/[\Delta H_i(M)+\Delta H_j(M-\Delta M_j)+\Delta H_i(M-\Delta M_j)+\Delta H_j(M-\Delta M_j+\Delta M_i)]$ defined for recoil curve pair (i,j). In mean field theory, $r_{ij}(M)=0$ and consequently $r=0$.[7] Therefore the value of $r_{ij}(M)$ or r just monitors the deviation from the mean-field approximaiton. r is obtained by averaging $r_{ij}(M)$ over a general set of multiple recoil curves. r can be considered as a quantitative measure that allows an accurate check of how close or far any $\Delta H(M,\Delta M)$ data set is from fulfilling the mean-field approximation. The specific advantage of this quantity r is that it can be directly calculated from data sets alone without the need for any data fitting. The results are shown in contour plots (Fig. 9).

1. Contour plots

The overall shape of the contour plots in the absence of interaction randomness has been qualitatively explained by the interaction *compensation* effect.[9] From the model Hamiltonian Eq. (10), we know that the intergranular exchange interactions are FM and short-range while the magnetostatic interactions are AFM and long-range. The competition between the two "opposite" interaction tendencies will yield a variety of system behaviors. The key point is that only when J_{ms} is comparable with J_{ex} can the magnetostatic and exchange interactions cancel most. Consequently, the system is most mean-fieldlike and the $\Delta H(M,\Delta M)$ method is most reliable there. This parameter range is called the interaction compensation region or equivalently the reliability range of the $\Delta H(M,\Delta M)$ method. Individually increasing either one will make the $\Delta H(M,\Delta M)$ method less reliable, while increasing both of them with proper strength ratio will substantially extend the reliability range. This explains why the overall contour shape is nearly symmetric along the direction with $J_{\mathrm{ms}}/J_{\mathrm{ex}}\sim$ constant. The slight tilt of the ellipse upwards results from the fact that only the nearest neighbor interactions are compensated, but not the total interaction fields. Due to its long-range nature, the total magnetostatic field actually dominates the exchange. However, due to the almost

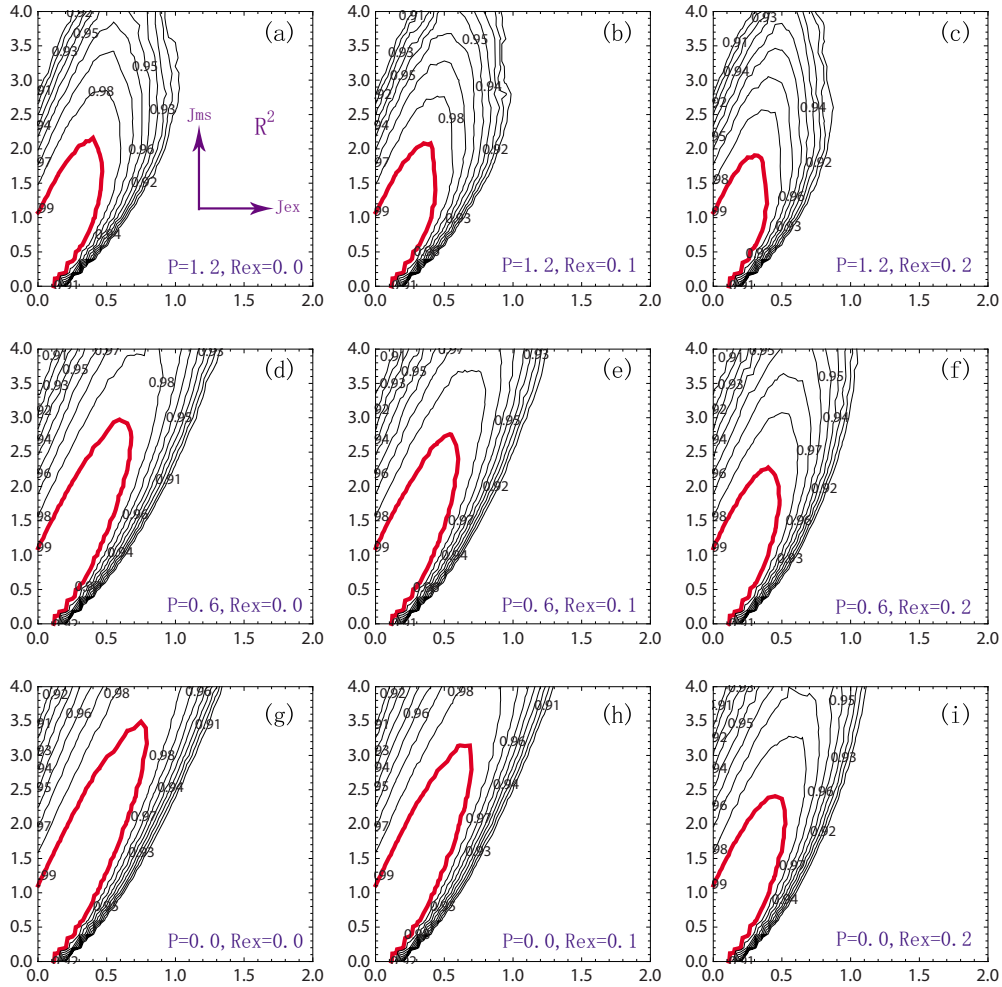

FIG. 8. (Color online) P and R_{ex} dependent contour plots of the reliability measure R^2. The critical contour with $R_c^2=0.99$ is marked with thick solid lines.

perfect suppression of the nearest neighbor interactions in this case, the correlation processes that produce deviations from the mean-field behavior are effectively suppressed. This suggests that the $\Delta H(M,\Delta M)$ method can clearly cope with higher magnetostatic interactions than exchange interactions, in agreement with previous micromagnetic tests.[5]

Upon looking at the resulting structures in Figs. 7–9, we notice that the overall contour shape is nearly symmetric along the $J_{ms}/J_{ex}=3$ direction. Note that in our previous study where the dipole approximation was used, we found the contour plot to be nearly symmetric along the $J_{dp}/J_{ex}=1$ direction. From the Eq. (3) we notice that if $J_{dp}/J_{ex}=1$, the exchange and dipolar interactions will cancel exactly for the nearest-neighboring grains, which have $\tilde{r}_{ij}=1$. This partially explains why the contour plot is nearly symmetric along the $J_{dp}/J_{ex}=1$ direction. In contrast to these earlier studies, we consider here the exact magnetostatic interaction (U_{ms}) instead of dipole interaction approximation (U_{dp}) for grains that are close to each other. In the case of $d/a=2$, our calculation demonstrates that the dipole approximation is rather unreliable with $U_{dp}/U_{ms}\approx 3$ for the nearest neighbor grains ($\tilde{r}_{ij}=1$). Correspondingly, J_{ms} needs to be about three times the size of J_{ex} to compensate the nearest neighbor grain interactions in the proper magnetostatic calculations. This explains why the contour is nearly symmetric along the $J_{ms}/J_{ex}=3$ direction.

Secondly, we find that with increasing randomness in the couplings, the reliability range shrinks slightly but in a well-defined fashion. To quantify the shrink, one can define a critical value for each reliability measure, above which this method is sufficiently accurate. For example, we might define $P_d^c=-0.04$, $R_c^2=0.99$, and $r_c=0.012$ to be the critical value for P_d, R^2, and r, respectively. These particular contours will be referred to as the critical contours, and marked with thick solid lines in our plots. We find that the areas of these critical contours keep decreasing upon increasing randomness in the exchange and magnetostatic couplings. Moreover, in the limit that $P=0$, i.e., uniform grain volumes and uniform magnetostatic couplings, the shrink of the critical contours upon increasing R_{ex} is faster than the $P>0$ cases. Similarly, in the limit that $R_{ex}=0$, i.e., no randomness in the exchange couplings, the shrink of the critical contours upon increasing P is faster than the $R_{ex}>0$ cases. This behavior can be understood as above using the interaction compensation effect argument. In the case of one interaction type being uniform, the probability of canceling the contributions from the nearest neighbor interactions is smaller than the case of both interaction types being random. Because even though the first moment contributions from exchange and magnetostatic interactions might be equal, the second and higher moments of the coupling constant distributions will not be. In other words exact cancellation for nearest neigh-

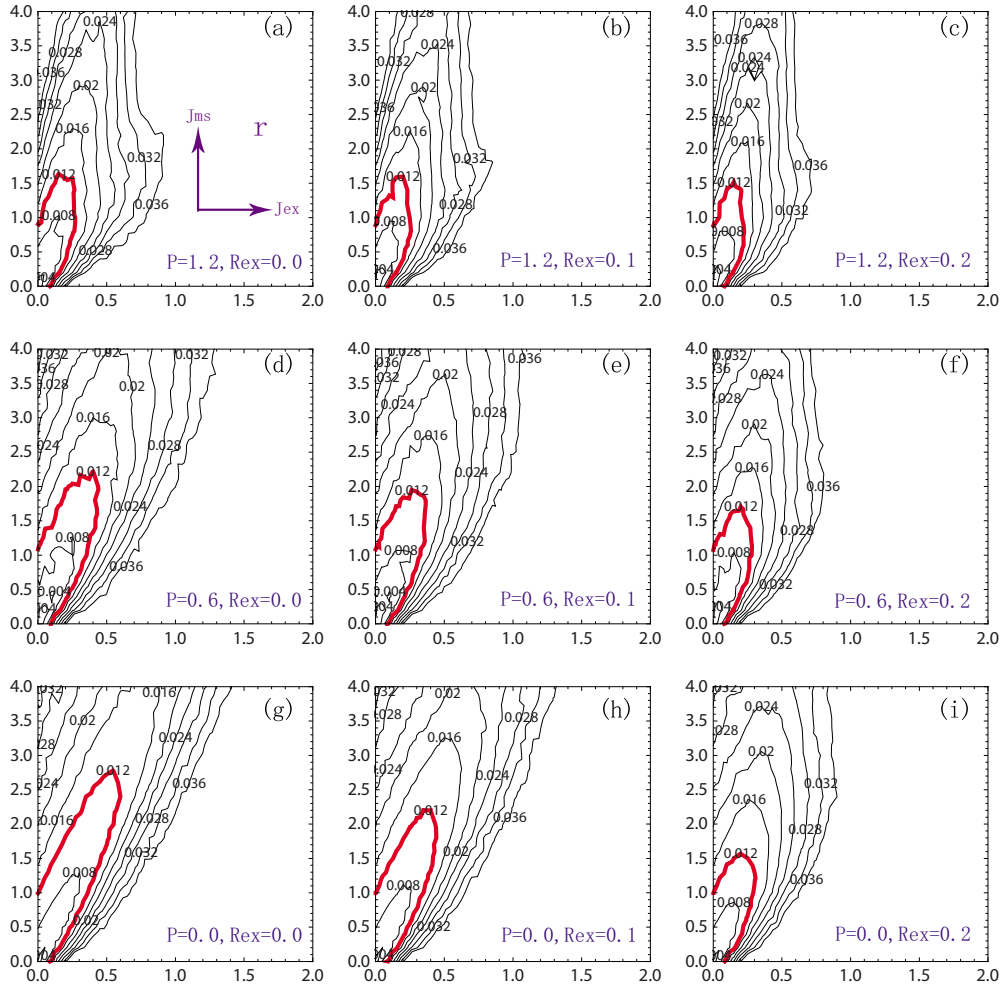

FIG. 9. (Color online) P and R_{ex} dependent contour plots of the reliability measure r. The critical contour with $r_c=0.012$ is marked with thick solid lines.

bors is very unlikely in this case. However, in case of random exchange and magnetostatic coupling constants, there exists a possibility for cancellation of even higher order moment contributions. Therefore, it is expected that the presence of randomness in both interaction types can actually improve performance of the $\Delta H(M,\Delta M)$ method compared to cases with either one interaction type being uniform.

2. Correlations

Overall, the contour plots of the three reliability measures show very similar features, which indicates that there could be correlations with each other. Moreover, as mentioned above, the deviation-from-redundancy measure r can be directly calculated from data sets alone without the need for any data fitting. Knowledge of a possible correlation between the fit-quality measure (either R^2 or P_d) and the deviation-from-redundancy measure r will enable the estimation of the suitability of the $\Delta H(M,\Delta M)$ method even without any data fitting. Considering this, we plot R^2 versus r, P_d versus r, and R^2 versus $-P_d$ for the complete data set of different $(P,R_{ex};J_{ms},J_{ex})$ (see Fig. 10). In order to show the trend more clearly, only three sets of (P,R_{ex}) are shown here.

From Fig. 10(a) or Fig. 10(b), we find that in the absence of random couplings, i.e., $(P,R_{ex})=(0,0)$, the data points fall onto a fairly well-defined curve, in the high R^2 or low $|P_d|$ range, where the utilization of the $\Delta H(M,\Delta M)$ method is sensible and accurate. This indicates that R^2 and P_d are highly correlated with r in the regime where these quantities matter, corroborating our earlier result.[9] One now has a criterion that enables a judgment on the usefulness and reliability of any $\Delta H(M,\Delta M)$-data set evaluation. In practice, one simply determines the r value from experimental or modeling data sets, looks up the expected precision with the help of the correlation plots Fig. 10 and then decides if a further data analysis is warranted or not. This procedure can be termed as the r-parameter quality control.

Upon adding randomness into J_{ex} and J_{ms} through increasing R_{ex} and P, the P_d versus r (or R^2 versus r) correlation is approximately preserved but the curve is slightly shifted to right. Also, the data spread has increased slightly as illustrated by the increasing error bars. This right shift in the r-dependence of the fit qualities simply reflects the fact that increasing R_{ex} and P causes an elevated level of redundancy suppression, even though the $\Delta H(M,\Delta M)$ method still works well and gives precise fit parameters. This right shift also means that the r-parameter quality control still works and produces an even more stringent quality control test in the presence of nonuniform couplings.

From Fig. 10(c), we find that the data points fall onto fairly well-defined curves in spite of the presence of nonuni-

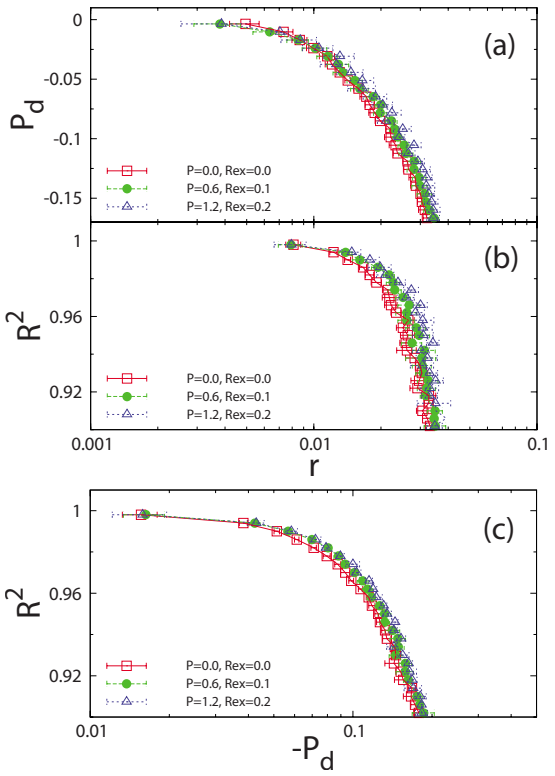

FIG. 10. (Color online) Correlations between the reliability measures: (a) P_d and r; (b) R^2 and r; (c) R^2 and $-P_d$. Data points with the same (P,R_{ex}) value are grouped and shown with the same symbol, as indicated by the legend. In these $Y(X)$-correlation plots, we calculate the average X values within linear Y-bins. The error bars present the 95% confidence interval, i.e., $\pm 2\sigma$.

form couplings. This indicates that R^2 and P_d are highly correlated with each other and this correlation is not affected by the randomness of couplings.

IV. CONCLUSION

In summary, we developed an interacting random hysteron model, which self-consistently accounts for the local variations of the exchange and magnetostatic interactions and their correlations with the geometrical distribution of grains in magnetic recording media. We used the so developed model to generate hysteresis loop data for different interaction magnitudes and different amounts of the randomness and performed an identification analysis aimed at extracting the intrinsic SFD from the hysteresis loops. The conventional $\Delta H(M,\Delta M)$-methodology has been used as an extraction tool. We find that, even in the presence of locally varying exchange and magnetostatic couplings, the SFD can be determined by means of the $\Delta H(M,\Delta M)$ method; however, with a somewhat reduced accuracy. The strong and robust correlations among the reliability measures gives a natural r-parameter quality control procedure, which can be utilized as a criterion to decide if a full scale data analysis is warranted, even in the case of nonuniform couplings.

ACKNOWLEDGMENTS

Y.L. and K.D. acknowledge support from NSF through Grant No. DMR 03-14279 and the Materials Computation Center Grant No. DMR 03-25939(ITR). Work at nanoGUNE acknowledges funding from the Department of Industry, Trade and Tourism of the Basque Government and the Provincial Council of Gipuzkoa under the ETORTEK Program, Project No. IE06-172, as well as from the Spanish Ministry of Science and Education under the Consolider-Ingenio 2010 Program, Project No. CSD2006-53. O.H. acknowledges support through the Marie Curie International Reintegration Grant within the 7th European Community Framework Programme, Project No. 224924.

APPENDIX: CALCULATE LONG-RANGE MAGNETOSTATIC INTERACTIONS

In our previous study, the Lekner formalism was used to deal with the long-range dipolar interactions within a periodic system.[9] All grains were considered as dipoles there. In calculating the long-range dipolar interaction between grain i and j, we have to take into account: (1) the dipolar interaction between grain i and j in the central simulation cell; (2) the dipolar interactions between grain i in the central simulation cell and all the images of grain j in the image cells. Therefore, the dipolar interaction energy must be calculated as

$$U_{\mathrm{dp}} = J_{\mathrm{dp}} \sum_{\substack{i\neq j \\ \text{all cells}}} \frac{S_i S_j}{\tilde{r}_{ij}^3} = J_{\mathrm{dp}} \sum_{i,j} S_i S_j \sum_{\boldsymbol{C}}{}' \frac{1}{|\tilde{\boldsymbol{r}}_{ij} + \tilde{\boldsymbol{C}}|^3}$$

$$\equiv J_{\mathrm{dp}} \sum_{i,j} S_i S_j \tilde{\mathcal{F}}_{ij}. \tag{A1}$$

Here the $\boldsymbol{C}$-sum is over all the simulation cells. The prime on the $\boldsymbol{C}$-sum indicates that it is over all images of grain j except $\boldsymbol{C}=0$ if $j=i$ because we assume that grain i interacts with all its periodic images, but not with itself. In the case that the central simulation cell is a 2D lattice with rhombus shape of angle ψ and side length $L=\tilde{L}a$, one has $\boldsymbol{C}=(l+\beta m,\gamma m)\tilde{L}a = \tilde{\boldsymbol{C}}a$ with l, m integers, $\beta=\cos\psi$, and $\gamma=\sin\psi$. The $\boldsymbol{C}$-sum can then be written as

$$\tilde{\mathcal{F}}_{ij} = \tilde{L}^{-3} \sum_{l,m=-\infty}^{\infty}{}' \frac{1}{[(\xi_{ij}+l+\beta m)^2 + (\eta_{ij}+\gamma m)^2]^{3/2}}, \tag{A2}$$

with $\xi_{ij}=(x_i-x_j)/L$ and $\eta_{ij}=(y_i-y_j)/L$. Here the prism indicates that we omit the $l=m=0$ term if $\xi_{ij}=\eta_{ij}=0$. $\tilde{\mathcal{F}}_{ij}\tilde{L}^3$ can be efficiently calculated with the Lekner formalism, which converts the slowly convergent summation to a rapidly convergent one

$$F(\xi,\eta) = \frac{2\pi^2}{\gamma^2 \sin^2(\pi\eta/\gamma)} + 8\pi \sum_{l=1}^{+\infty} \sum_{m=-\infty}^{+\infty} \cos[2\pi l(\xi+\beta m)]$$

$$\times \frac{l}{|\eta+\gamma m|} K_1(2\pi l|\eta+\gamma m|), \tag{A3}$$

or

$$F(\xi,\eta)=\frac{2\pi^2}{\gamma^2\sin^2(\pi\xi'/\gamma)}+8\pi\sum_{m=1}^{+\infty}\sum_{l=-\infty}^{+\infty}\cos[2\pi m(\eta'+\beta l)]\times\frac{m}{|\xi'+\gamma l|}K_1(2\pi m|\xi'+\gamma l|), \tag{A4}$$

with $\eta'=\gamma\xi-\beta\eta$, $\eta'=\beta\xi+\gamma\eta$, and $K_\nu(z)$ is the modified Bessel function of the second kind.[12,13]

Similarly, in the magnetostatic picture, the magnetostatic energy of the periodic system has to be calculated as

$$\begin{aligned}U_{\mathrm{ms}}&=\sum_{\substack{i\neq j\\ \text{all cells}}}\frac{1}{2}S_iS_jM_0^2\mathcal{I}(\boldsymbol{r}_i,\boldsymbol{r}_j;d)\\&=\sum_{\substack{i\neq j\\ \text{all cells}}}\frac{1}{2}S_iS_jM_0^2a^3\mathcal{I}(\tilde{\boldsymbol{r}}_i,\tilde{\boldsymbol{r}}_j;\tilde{d})\\&=\sum_{i,j}\frac{1}{2}S_iS_jM_0^2a^3{\sum_{\boldsymbol{C}}}'\mathcal{I}(\tilde{\boldsymbol{r}}_i,\tilde{\boldsymbol{r}}_j+\tilde{\boldsymbol{C}};\tilde{d}),\end{aligned} \tag{A5}$$

with $\tilde{d}=d/a$. At first glance, the $\boldsymbol{C}$-sum here is extremely complicated due to the four-dimensional integrals $\mathcal{I}(\tilde{\boldsymbol{r}}_i,\tilde{\boldsymbol{r}}_j+\tilde{\boldsymbol{C}};\tilde{d})$. However, as discussed in Sec. II C, if $r_{ij}\geq r_c$, these integrals can be calculated with the dipole approximation very well. Only when $r_{ij}<r_c$, shall we deal with the integrals explicitly. Fortunately, this does not happen too often. As long as $r_c\leq L/2$, it is easy to show that for grain i and grain j (and all grain j images), if there is one pair which fulfills $r<r_c$, then this is the only pair. Because grain j and all its images are separated by at least distance L. (This proof is very similar to that of the "minimum image criterion" used in the molecular dynamics simulation.) Therefore, we can easily correct the dipole approximation

$${\sum_{\boldsymbol{C}}}'\mathcal{I}(\tilde{\boldsymbol{r}}_i,\tilde{\boldsymbol{r}}_j+\tilde{\boldsymbol{C}};\tilde{d})={\sum_{\boldsymbol{C}}}'\frac{\tilde{A}_i\tilde{A}_j\tilde{d}^2}{|\tilde{\boldsymbol{r}}_{ij}+\tilde{\boldsymbol{C}}|^3}-\frac{\tilde{A}_i\tilde{A}_j\tilde{d}^2}{\tilde{r}_{ij_{\min}}^3}+\mathcal{I}(\tilde{\boldsymbol{r}}_i,\tilde{\boldsymbol{r}}_{j_{\min}};\tilde{d}), \tag{A6}$$

with $\tilde{A}_i=A_i/a^2$ and $\tilde{A}_j=A_j/a^2$. The first term, i.e., the dipole approximation, can be calculated within the Lekner formalism. The rest is the correction and can be easily calculated. Note that $j_{\min}$ denotes the minimal image of grain j which satisfies $r_{ij_{\min}}<r_c$. For some pairs of grains, there are no such minimal images at all, which means we can safely use the dipole approximation without corrections. Otherwise, we just use Eq. (A6) to calculate the magnetostatic interaction. In all cases, this can be done in advance and saved into a file for future use in the calculation of $M(H)$ curves.

It is useful to combine Eqs. (A5) and (A6) to derive

$$U_{\mathrm{ms}}=\sum_{i,j}J_{\mathrm{ms}}^{ij}S_iS_j\tilde{\mathcal{F}}'_{ij}, \tag{A7}$$

with

$$\tilde{\mathcal{F}}'_{ij}\equiv\tilde{\mathcal{F}}_{ij}-\frac{1}{\tilde{r}_{ij_{\min}}^3}+\frac{1}{\tilde{A}_i\tilde{A}_j\tilde{d}^2}\mathcal{I}(\tilde{\boldsymbol{r}}_i,\tilde{\boldsymbol{r}}_{j_{\min}};\tilde{d}). \tag{A8}$$

Comparing Eq. (A7) with Eq. (A1), one can easily see the modification we have done so far. In the limit that there is no microstructural disorder, one has $J_{\mathrm{ex}}^{ij}=J_{\mathrm{ex}}$, $\tilde{v}_i=1$, and $J_{\mathrm{ms}}^{ij}=J_{\mathrm{ms}}$. Furthermore, if dipole approximation is used then $J_{\mathrm{ms}}=J_{\mathrm{dp}}$ and we have $\tilde{\mathcal{F}}'_{ij}=\tilde{\mathcal{F}}_{ij}$, i.e., the original Hamiltonian Eq. (3) is recovered from Eq. (10).

[1] Y. Shimizu and H. N. Bertram, IEEE Trans. Magn. **39**, 1846 (2003).
[2] A. Berger, Y. H. Xu, B. Lengsfield, Y. Ikeda, and E. E. Fullerton, IEEE Trans. Magn. **41**, 3178 (2005).
[3] S. J. Greaves, A. M. Goodman, H. Muraoka, and Y. Nakamura, J. Magn. Magn. Mater. **287**, 66 (2005).
[4] J. Miles, IEEE Trans. Magn. **43**, 955 (2007).
[5] A. Berger, B. Lengsfield, and Y. Ikeda, J. Appl. Phys. **99**, 08E705 (2006).
[6] O. Hellwig, A. Berger, T. Thomson, E. Dobisz, Z. Z. Bandic, H. Yang, D. S. Kercher, and E. E. Fullerton, Appl. Phys. Lett. **90**, 162516 (2007).
[7] Y. Liu, K. A. Dahmen, and A. Berger, Phys. Rev. B **77**, 054422 (2008).
[8] Y. Liu, K. A. Dahmen, and A. Berger, J. Appl. Phys. **103**, 07F504 (2008).
[9] Y. Liu, K. A. Dahmen, and A. Berger, Appl. Phys. Lett. **92**, 222503 (2008).
[10] A. E. LaBonte, J. Appl. Phys. **40**, 2450 (1969).
[11] M. Schabes and A. Aharoni, IEEE Trans. Magn. **23**, 3882 (1987).
[12] J. Lekner, Physica A **176**, 485 (1991).
[13] A. Grzybowski and A. Bródka, Mol. Phys. **100**, 1017 (2002).